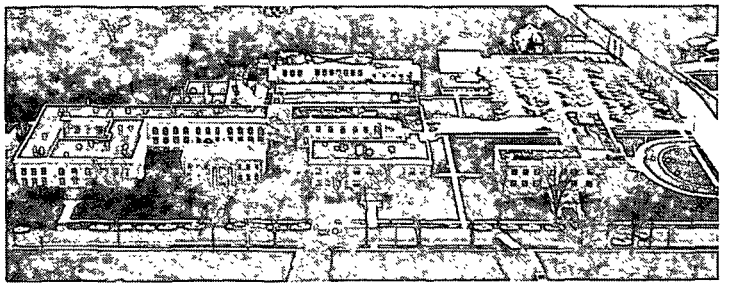

THE INSTITUTE OF PAPER CHEMISTRY, APPLETON, WISCONSIN

IPC TECHNICAL PAPER SERIES

NUMBER 314

AN IMPROVED THEORY OF CHAR BURNING

D. W. SUMNICHT AND T. M. GRACE

DECEMBER, 1988

An Improved Theory of Char Burning

D. W. Sumnicht and T. M. Grace

Portions of this work were used by DSW as partial fulfillment of the requirements for the Ph.D. degree at The Institute of Paper Chemistry. This manuscript has been submitted for consideration for publication in the Journal of Pulp and Paper Science

ABSTRACT

An improved model of char burning has been developed which includes direct carbon oxidation, carbon gasification with carbon dioxide, and the sulfate-sulfide cycle. This more realistic model lessens the need to postulate high burning temperatures in order to match experimental burning times and maintain high reduction efficiencies during the burn. By including a moderate fuming rate during char burning, the model is able to match an experimental mass-time curve very closely. The improved model clearly shows that oxidation of char carbon with oxygen and sulfate reduction do occur simultaneously during char burning.

AN IMPROVED THEORY OF CHAR BURNING

D. W. Sumnicht and T. M. Grace
The Institute of Paper Chemistry
Appleton, WI 54912

INTRODUCTION

Kraft black liquor combustion proceeds through several stages which are fairly distinct: drying, pyrolysis, and char combustion (1). Drying removes the water and pyrolysis produces volatile organic compounds, leaving fixed carbon, a small amount of fixed hydrogen, and inorganic alkali salts. This residual mixture is referred to as char, and the organic carbon in the char is referred to as char carbon. Char combustion is the slowest stage of black liquor combustion and may not be completed during the flight of the particle in the recovery furnace. In such a case, the particle may eventually fall onto the char bed at the bottom of the furnace where combustion of char carbon is completed. During char combustion, sodium sulfate (Na_2SO_4) is reduced to the active pulping chemical sodium sulfide (Na_2S).

The simultaneous oxidation of char carbon and reduction of Na_2SO_4 is described by the sulfate/sulfide cycle theory of char burning. The sulfate/sulfide cycle was first identified in molten sodium carbonate melts by Gehri and Oldenkamp (2) and later applied to kraft char burning by Grace et al. (3). The cycle is depicted in Figure 1. Oxygen reacts with sodium sulfide (Na_2S) to produce sodium sulfate (Na_2SO_4) which in turn reacts with carbon to produce a mixture of carbon monoxide (CO) and carbon dioxide (CO_2); sodium sulfide is regenerated in the reaction between carbon and sodium sulfate. In the sulfate/sulfide cycle, the only pathway for carbon consumption is the C/Na_2SO_4 reaction, and the only source of oxygen for the Na_2S/O_2 reaction is oxygen from the combustion air. The relative amounts of sulfide and sulfate

depend on the relative rates of the Na_2S/O_2 and C/Na_2SO_4 reactions. Sulfide predominates over sulfate while carbon is burned if the rate-limiting step is the Na_2S/O_2 reaction or oxygen mass transfer; it is therefore possible to have sulfide be the dominant sulfur species as char carbon is burned in air.

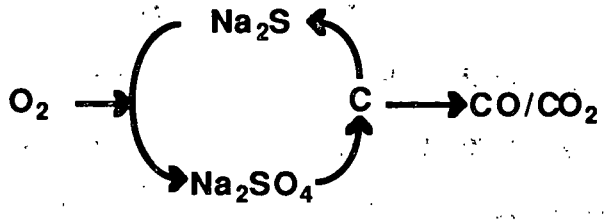

Figure 1. Sulfate - sulfide cycle.

The sulfate/sulfide cycle can be treated quantitatively if the rates are known for each reaction. Equation (1) is a carbon balance on a discrete quantity of char:

$$-\frac{d[C]}{dt} = \frac{4}{2-f} R_{CS} \qquad (1)$$

where

[C] = carbon concentration, mole C/mole Na_2
R_{CS} = C/Na_2SO_4 reaction rate, mole Na_2SO_4/mole Na_2-sec
f = molar $CO/(CO + CO_2)$ ratio

The $\frac{4}{2-f}$ term in Equation (1) specifies that four moles of carbon are consumed per mole of sulfate if the product of the C/Na_2SO_4 reaction is all CO (f=1), and two moles of carbon are consumed if all CO_2 (f=0) is produced. Equation (2) is a sulfide balance:

$$\frac{d[Na_2S]}{dt} = s\frac{dr}{dt} = R_{CS} - R_{SO} \qquad (2)$$

where

$[Na_2S]$ = sulfide concentration, mole Na_2S/mole Na_2
R_{CS} = C/Na_2SO_4 reaction rate, mole Na_2SO_4/mole Na_2-sec
R_{SO} = sulfide oxidation rate, mole Na_2S/mole Na_2-sec
r = "reduction efficiency" = molar $Na_2S/(Na_2S + Na_2SO_4)$ ratio
s = moles sulfur/mole Na_2

Equations (1) and (2) describe the rate of char carbon consumption and the net oxidation state of the sulfur species.

Grace et al. developed an expression for R_{CS} and determined that R_{SO} was mass-transfer limited in molten smelt until nearly all the sulfide was oxidized (3). Thus, R_{SO} is just an appropriate mass-transfer rate for the geometry being considered. R_{CS} was measured in a smelt pool reactor where molten inorganic salts were present in great excess. Equations (1) and (2) were used to simulate the combustion of a single kraft char particle to see if the C/Na_2SO_4 rate measured in the smelt pool reactor at low carbon concentrations could be extended to char burning where much more carbon is normally present. The application of the sulfate/sulfide cycle to the burning of single char particles was successful at predicting the general trends seen including:

1.) a period where the weight loss rate is constant;
2.) weight gain near the end of combustion due to sulfide reoxidation;
3.) an apparently high reduction efficiency during burning as manifested by the reoxidation of sulfide at the end of the burn.

On the other hand, a couple of weaknesses are apparent:

1.) only one pathway for carbon consumption is provided;
2.) extremely high temperatures need to be hypothesized.

The provision of only one pathway for char carbon consumption is incomplete. Other possible reactions involving carbon include:

$$C + \frac{1}{2}O_2 \rightarrow CO \quad (3)$$

$$C + O_2 \rightarrow CO_2 \quad (4)$$

$$C + CO_2 \rightarrow 2CO \quad (5)$$

$$C + H_2O \rightarrow CO + H_2 \quad (6)$$

The sulfate/sulfide cycle was identified in molten carbonate systems, so it applies to regions where smelt is in intimate contact with the carbon. In such a case, oxygen reacts with sulfide in the smelt, and the sulfate product reacts with carbon. The char carbon, however, is not necessarily covered by smelt, and it is possible for the char carbon to react directly with the gases flowing over the char. Thus, reactions (3) - (6) can operate simultaneously with the sulfate/sulfide cycle.

Another weakness of the application of the sulfate/sulfide cycle to char burning is the need to hypothesize an extremely high reaction temperature. Char bed temperatures are in the range of 1200 - 1400 K, and char particle temperatures have been measured as high as 1473 K (1). The sulfate/sulfide cycle theory of char burning, however, requires reaction temperatures as high as 1600 K for two reasons. Firstly, a high temperature is necessary to predict a fast enough C/Na_2SO_4 rate to match experimental particle burning rates. Secondly, a high temperature is necessary to maintain a high reduction efficiency until near the end of the particle burn. The high temperature causes sulfide in the char particle to predominate over sulfate until near the end of the burn when sulfide is reoxidized, causing the particle to gain weight. At temperatures lower than 1600 K, Grace's equations predict net oxidation of the sulfide early in the particle burn instead of the experimentally observed oxidation of sulfide near the end of the burn.

The sulfate/sulfide cycle operates when the oxygen gas reacts with char carbon via liquid smelt, but there are at least two possible modes of gas/char-carbon contact. As a char particle burns, you can see small regions of molten inorganic salts ("smelt") that have coalesced out of the greater particle; yet, other regions that appear carbonaceous coexist with the molten regions. The possibility exists for gas/solid interactions as well as gas/liquid interactions.

Other carbon gasification reactions should be included in the

sulfate/sulfide cycle to make a more general theory of char burning. Reactions (3) - (6) are potential pathways for carbon consumption in addition to the C/Na_2SO_4 reaction.

IMPROVED THEORY OF CHAR BURNING

This paper describes a revised theory of char burning that takes the carbon/oxygen and carbon/CO_2 reactions into account. Equation (1) is modified to include these reactions:

$$-\frac{d[C]}{dt} = \frac{4}{2 - f_{cs}} R_{CS} + \frac{2}{2 - f_{cox}} R_{COX} + R_{CO_2} \qquad (7)$$

where

[C] = carbon concentration, mole C/mole Na_2
R_{CS} = C/Na_2SO_4 reaction rate, mole Na_2SO_4/mole Na_2-sec
R_{COX} = C/O_2 reaction rate, mole O_2/mole Na_2-sec
R_{CO_2} = C/CO_2 reaction rate, mole C/mole Na_2 -sec
f_{cs} = molar $CO/(CO + CO_2)$ ratio for the carbon/sulfate reaction
f_{cox} = molar $CO/(CO + CO_2)$ ratio for the carbon/oxygen reaction

Equation (2), the sulfide balance, remains the same.

Equations (2) and (7) represent a quantitative treatment of the combustion of a discrete quantity of char, provided that appropriate rate equations are available. The next step in the development of the model is to choose representative rate equations for R_{CS}, R_{COX}, R_{SO}, and R_{CO2}.

Rate equation for the C/Na_2SO_4 reaction

Rate expressions have been developed for the C/Na_2SO_4 reaction in a molten carbonate melt for different types of carbon. A smelt pool reactor was used by researchers at The Institute of Paper Chemistry (IPC) (3). The reactor consists of a crucible which is heated to a set temperature by an induction furnace. Small quantities of char are placed in a smelt and the sulfate/sulfide

cycle is active when an oxygen-containing gas is bubbled through the smelt. The system relies on the bubbling action for mixing the char/smelt mixture. The sulfide oxidation was found to be a very fast, mass-transfer-controlled reaction in this system. The rate expression for the C/Na_2SO_4 reaction takes the following form:

$$R_{CS} = -k_1 \left\{ \frac{[SO_4]}{k_2 + [SO_4]} \right\} [C]\, e^{\frac{-E}{RT}} = -k_1 \left\{ \frac{(1-r)\,s}{k_2 + (1-r)\,s} \right\} [C]\, e^{\frac{-E}{RT}} \qquad (8)$$

where

$[SO_4]$ = sulfate concentration, mole sulfate/mole Na_2
$[C]$ = carbon concentration, mole C/mole Na_2
k_1, k_2 = rate constants
E = activation energy
R = gas constant
T = absolute temperature

Table 1 contains the rate constants for different types of carbon in batch experiments with great excess of molten salt.

Table 1. IPC rate parameters for carbon-sulfate reaction.

Carbon type	k_1, sec^{-1}	k_2, $\frac{\text{mole } SO_4}{\text{mole } Na_2}$	E, $\frac{cal}{mole}$
Kraft char	$1.31 \pm 0.41 \times 10^3$	0.0011 ± 0.0004	$29{,}200 \pm 1{,}000$
Pulverized graphite	$4.94 \pm 0.82 \times 10^4$	0.0013 ± 0.0003	$44{,}000 \pm 1{,}200$
Soda char	$3.04 \pm 0.73 \times 10^5$	0.0020 ± 0.0006	$39{,}850 \pm 1{,}500$

The C/Na_2SO_4 reaction was also studied by Thorman and Macur using activated carbon (5). They also used a molten-salt reactor, but mixing was performed using a turbine blade agitator rather than relying on the mixing action of the bubbles. The turbine allowed them to investigate higher carbon loadings than the IPC system. Thorman and Macur's rate expression takes the following form:

$$-\frac{d[SO_4]}{dt} = A[C]^n e^{\frac{-E}{RT}} \quad (9)$$

where

$A = 1.67 \pm 0.15 \times 10^8$ g$^{0.69}$ min^{-1} 100 g solution$^{-0.69}$
E = activation energy = $2.04 \pm 0.15 \times 10^5$ J/gmole
n = reaction order = 0.31 ± 0.02

Thorman and Macur investigated the reaction in the temperature range of 1200 - 1300 K and carbon concentrations in the range of 1 - 3.6 mole C/mole Na_2. The IPC data were obtained at temperatures between 1060 - 1230 K and carbon concentrations on the order of 0.02 mole C/mole Na_2.

The predicted IPC rate is compared to the predicted Thorman and Macur (T&M) rate in Table 2 at various conditions. The IPC rate for kraft char is predicted to be substantially greater than the T&M rate using activated carbon. On the other hand, the IPC rate for pulverized graphite is much closer to the T&M rate using activated carbon. The difference in rates between the IPC kraft char and the T&M activated carbon may possibly be explained by the difference between the inherent reactivity of activated carbon and char.

Table 2. Relative rate for the carbon/sulfate reaction.

T K	[C] $\frac{\text{mole C}}{\text{mole } Na_2}$	$\frac{\text{IPC char rate}}{\text{T\&M rate}}$	$\frac{\text{IPC graphite rate}}{\text{T\&M rate}}$
1200	0.03	10	0.73
1200	0.3	46	3.5
1200	3	190	14
1600	0.03	1	0.45
1600	0.3	6	2.2
1600	3	25	8.9

The problems of applying the sulfate/sulfide cycle to char burning would be exacerbated by using the slower rate predicted by Thorman and Macur's rate

equation. Experimental single particle burns indicate that a high reduction efficiency is maintained until near the end of the burn (3). This experimental observation required Grace to hypothesize a reaction temperature as high as 1600 K in simulated single particle burns so that the IPC rate equation would predict a C/Na_2SO_4 rate which was fast enough to maintain a high reduction efficiency. It is apparent from Table 2 that an unreasonably high temperature would have to be hypothesized if the T&M rate equation were used. Thus, the IPC rate equation for kraft char is most applicable to the char-burning model considered in this paper.

Rate equation for the C/O_2 reaction

An appropriate rate equation for the carbon/oxygen reaction must be chosen. There are IPC weight loss data for combustion of soda char particles, but a rate equation has not been developed. It is possible, however, to borrow the mathematical form of the rate equation from the coal literature, and match the soda char rate to the coal char rate. The coal literature has data for coal of varying reactivities, but a given coal char and kraft char carbon may or may not have similar reaction rates. A rate expression from the coal literature must be chosen to match the observed rate of the carbon/oxygen reaction in soda char.

A first-order rate constant expression for a bituminous coal char taken from Smoot and Smith (4) is:

$$k_r[=]\frac{cm}{s} = 236\, T_g\, e^{\left(\frac{-11022}{T_p}\right)} \qquad (10)$$

where

T_g = gas temperature
T_p = particle temperature

For an irreversible heterogeneous reaction which is first order in oxygen concentration, the rate of oxygen consumption is K^*C_{BO} where the reaction constant K is comprised of the mass-transfer resistance and chemical

reaction resistance in series (6). The mass-transfer coefficient, k_m, and chemical reaction constant, k_r, make up K as follows:

$$K = \frac{1}{\frac{1}{k_m} + \frac{1}{k_r}} \tag{11}$$

Equation (10) shows the kinetic rate constant, and the mass-transfer coefficient is calculated using the Ranz correlation for one-dimensional flow past spheres (7).

$$Sh = \frac{k_m d}{D} = 2.0 + 0.6\, Re^{\frac{1}{2}}\, Sc^{\frac{1}{3}} \tag{12}$$

where

d = particle diameter
D = diffusivity
ν = kinematic viscosity
Re = Reynolds number = $\langle v \rangle d/\nu$
Sc = Schmidt number = ν/D.

Figure 2 shows that the carbon oxidation rate for coal char does an adequate job of predicting soda char burning rates. The circles represent the actual data for a soda char burn while the lines are the predicted curves for 1300, 1400, and 1500 K. The effect of a range of temperatures is shown since the actual particle temperature was not measured. The indicated temperatures were assumed to be both the particle and gas temperatures. Note that soda char was used rather than kraft char so that the sulfate/sulfide cycle would not be occurring in parallel with the carbon/oxygen reaction. There is always residual carbon at the end of a soda char burn, so the ultimate weight loss is not as great as if burnout was complete. The model in this case assumes a constant temperature throughout the burn, but the heat of reaction near the

end of a soda char burn is not great enough to keep a high reaction temperature, so reaction essentially stops before the carbon is completely burned. The difference in the ultimate weight loss may also be caused by possible differences between the assumed and actual char composition. The data where weight loss occurs is fit well by the predicted curve, so the expression chosen for the kinetic rate constant is adequate for use in the model.

Figure 2. Predicted soda char rates using coal data.

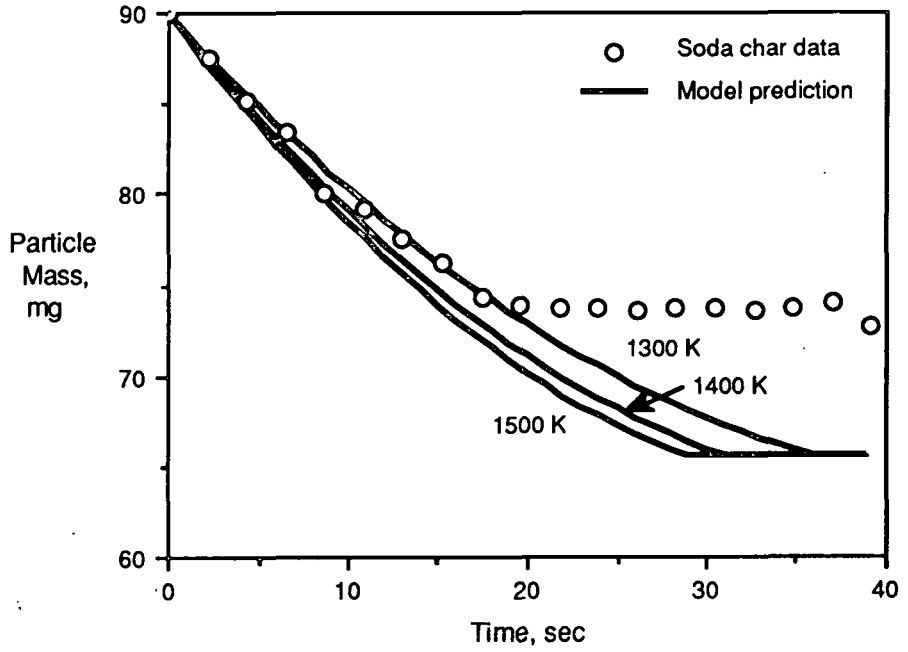

Rate equation for the C/CO_2 reaction

The C/CO_2 reaction was studied by Goerg (8) at very low carbon concentration and by Li (9) at high carbon concentration. Li's data span the range of 1.2 - 5.8 mole C/mole Na_2 while Goerg's data span the range of 0.015 - 0.062 mole C/mole Na_2 . Li's data were taken in the temperature range of 973 - 1048 K to avoid mass-transfer interferences while Goerg's data were

taken in the range of 1200 - 1283 K. Thus, Li's equation must be extrapolated to higher temperature while Goerg's equation must be extrapolated to higher carbon content to match the conditions found during char burning in the recovery furnace. When their rate expressions are put in the same units, they take the following form:

$$R_{CO_2} = \frac{-k_1 P_{CO_2}[C]}{1 + k_2 P_{CO_2} + k_3 P_{CO}} e^{\frac{-E}{RT}} \qquad (13)$$

The values of the constants are found in Table 3. Li's original equation had to be converted to the form found in Table 3.

Table 3. Values for C/CO_2 rate equation.

Parameter	Goerg	Li
k_1	1.043×10^8 $(atm\text{-}sec)^{-1}$	9.53×10^7 $(atm\text{-}sec)^{-1}$
k_2	28.99 atm^{-1}	10.8 atm^{-1}
k_3	45.6 atm^{-1}	6.3 atm^{-1}
E	227,300 J/mole	187,000 J/mole

The inhibitory effect of CO and CO_2 is stronger in Goerg's data than Li's. This may be partly due to the different temperatures at which the experiments were performed. The different activation energies have the biggest effect on the calculated rate. Goerg's activation energy is 21% greater than Li's, which causes Li's exponential term to be 40 times greater at 1300 K. The overall result is that Li's predicted rate is two orders of magnitude greater than Goerg's predicted rate at 1300 K. The rate discrepancy may be due to the different modes of C/CO_2 contact. The CO_2 in Goerg's system must interact with smelt before reacting with the carbon whereas the CO_2 in Li's system can react directly with carbon. Li's system is more representative of a burning char particle than Goerg's, so Li's constants will be used in the model considered in this paper.

Rate equation for the Na_2S/O_2 reaction

Consider the Na_2S/O_2 reaction rate, defined as R_{SO}. R_{SO} can be equated to both the mass-transfer rate and the chemical reaction rate as follows:

$$R_{SO} = k_m (C_{BO} - C_{S_{(1-P)}}) A (1-P) = k_{R_{so}} C_{S_{(1-P)}} A (1-P) \quad (14)$$

where

R_{SO} = sulfide oxidation rate
A = external area of the particle
C_{BO} = bulk oxygen concentration
$C_{S_{(1-P)}}$ = oxygen concentration at the liquid surface
k_m = mass transfer coefficient
k_{Rso} = kinetic rate coefficient
P = fraction of the external surface that is solid carbon

The parameter "P" determines the fraction of the oxygen in the air which reacts with the solid carbon. The value of (1-P) is therefore the fraction which reacts with the liquid smelt. The functionality of P will be discussed in the next section.

Solving Equation (14) for $C_{S_{(1-P)}}$ and substituting back in, R_{SO} is found to be:

$$R_{SO} = K_{SO} C_{BO} A (1-P) \quad (15)$$

where K_{SO} is defined by Equation (11). A similar analysis for the C/O_2 reaction rate, R_{COX}, gives the same form with (1-P) replaced with P:

$$R_{COX} = K_{COX} C_{BO} A P \quad (16)$$

The oxidation of sulfide was found to be controlled by mass-transfer under most circumstances (3); it is therefore valid to assume that $k_{Rso} >> k_m$ for the sulfide oxidation reaction over the temperature range of char combustion at all mass transfer rates. Thus, K_{SO} is assumed to be equal to the mass-transfer coefficient, k_m, for sulfide oxidation, so the sulfide oxidation rate is just a fraction of the rate of oxygen transfer to the char. A factor of two is

introduced into the R_{SO} term of the sulfide balance since it takes two moles of oxygen per mole of sulfide to get one mole of sulfate.

A quantitative model of char burning can be constructed from the selected rate equations. The arbitrary selection of a value for the f parameter introduced in Equation (1) can be eliminated by assuming that the product of the char/oxygen and char/sulfate reactions is CO_2. The relative amounts of CO and CO_2 are then determined by the relative rates of the CO_2-producing reactions and the C/CO_2 reaction.

Given the appropriate equations for the C/Na_2SO_4, C/O_2, C/CO_2, and Na_2S/O_2 rates, the quantitative treatment of char combustion becomes:

$$-\frac{d[C]}{dt} = 2620\left\{\frac{(1-r)\,s}{0.0011+(1-r)\,s}\right\}[C]\,e^{\frac{-14,696}{T}} + K_{COX}\,C_{BO}\,A\,P + \frac{9.53 \times 10^7\,P_{CO_2}[C]}{1+10.8\,P_{CO_2}+6.3\,P_{CO}}\,e^{\frac{-22,492}{T}} \qquad (17)$$

$$\frac{dr}{dt} = \frac{1310}{s}\left\{\frac{(1-r)\,s}{0.0011+(1-r)\,s}\right\}[C]\,e^{\frac{-29,200}{RT}} - \frac{k_m}{2\,s}\,C_{BO}\,A\,(1-P) \qquad (18)$$

Equations (17) and (18) can be used to simulate single particle combustion in order to compare the predictions of the model with actual char combustion data. Equations (17) and (18) are two ordinary differential equations which can be solved simultaneously for the carbon concentration and reduction efficiency. Since carbon loss and net oxygen gain/loss are assumed to be the only contributors to weight change for the moment, the particle mass can be calculated as combustion proceeds.

Partition of oxygen between the solid and liquid surfaces

Part of the oxygen from air will react directly with carbon, and part will react with carbon via the sulfate/sulfide cycle. The partition of the oxygen between these two pathways will depend on the fraction of the particle surface which is solid carbon and that fraction which is liquid smelt. The solid fraction of the surface area is assumed to be carbon which reacts directly with oxygen, and the liquid fraction is a smelt/carbon mixture that reacts with oxygen via the sulfate/sulfide cycle. The fraction will change as the combustion proceeds. Let "P" be defined as the fraction of the surface area which has gas/solid contact:

$$P = \frac{A_C}{A_C + A_I} \tag{19}$$

where

A_C = surface area of carbon
A_I = surface area of molten smelt

In spheres, the external surface area is proportional to the 2/3 power of volume. If the same relationship is assumed in the function of P, then

$$P = \frac{V_C^{\frac{2}{3}}}{V_C^{\frac{2}{3}} + V_I^{\frac{2}{3}}} \tag{20}$$

where

V_C = volume of carbon
V_I = volume of inorganic

Substituting in m/ρ for the volume and rearranging the terms gives

$$P = \frac{\left(\frac{m}{\rho}\right)_C^{\frac{2}{3}}}{\left(\frac{m}{\rho}\right)_C^{\frac{2}{3}} + \left(\frac{m}{\rho}\right)_I^{\frac{2}{3}}} = \frac{m_C^{\frac{2}{3}}}{m_C^{\frac{2}{3}} + \left(\frac{\rho_C m_I}{\rho_I}\right)^{\frac{2}{3}}} = \frac{\left(\frac{m_C}{m_{C0}}\right)^{\frac{2}{3}}}{\left(\frac{m_C}{m_{C0}}\right)^{\frac{2}{3}} + \left(\frac{\rho_C m_I}{\rho_I m_{C0}}\right)^{\frac{2}{3}}} = \frac{\left(\frac{[C]}{[C]_0}\right)^{\frac{2}{3}}}{\left(\frac{[C]}{[C]_0}\right)^{\frac{2}{3}} + \left(\frac{\rho_C m_I}{\rho_I m_{C0}}\right)^{\frac{2}{3}}} \tag{21}$$

where [C] is the carbon concentration and the subscripts "C", "I", and "0" denote char carbon, inorganic salts, and initial condition, respectively. Thus, P has a value less than one at the start of combustion and decreases nonlinearly to zero at the end of combustion.

The magnitude of P is determined by the char composition and the relative densities of smelt and char carbon. Grace analyzed several chars and concluded that the char composition could be simplified to a few species (3). Based on Grace's method for simplifying the composition, the kraft char used in the experimental particle burns can be assumed to have the char composition shown in Table 4.

Table 4. Simplified char composition.

	mole/mole Na_2
Carbon	3.50
Na_2S	0.06
Na_2SO_4	0.06
Na_2CO_3	0.88

Smelt and amorphous carbon both have a density of about 2 g/cc; if these values are plugged into Equation (21), along with the ratio of m_I to m_C determined from Table 4, P becomes

$$P = \frac{\left(\frac{[C]}{[C]_0}\right)^{\frac{2}{3}}}{\left(\frac{[C]}{[C]_0}\right)^{\frac{2}{3}} + 1.86} \qquad (22)$$

On the other hand, if the void fraction is assumed to be located in a carbon matrix while the inorganic components are considered separate from the matrix, then ρ_C would have a value for the density of char rather than the density of carbon alone. In such a case, if a density of 0.2 g/cc is assumed for the "char carbon" density, P becomes

$$P = \frac{\left(\frac{[C]}{[C]_0}\right)^{\frac{2}{3}}}{\left(\frac{[C]}{[C]_0}\right)^{\frac{2}{3}} + 0.4} \qquad (23)$$

Figure 3 shows Equations (22) and (23) which describe how P varies as combustion proceeds.

Figure 3. Fraction of surface area that is carbon as combustion proceeds.

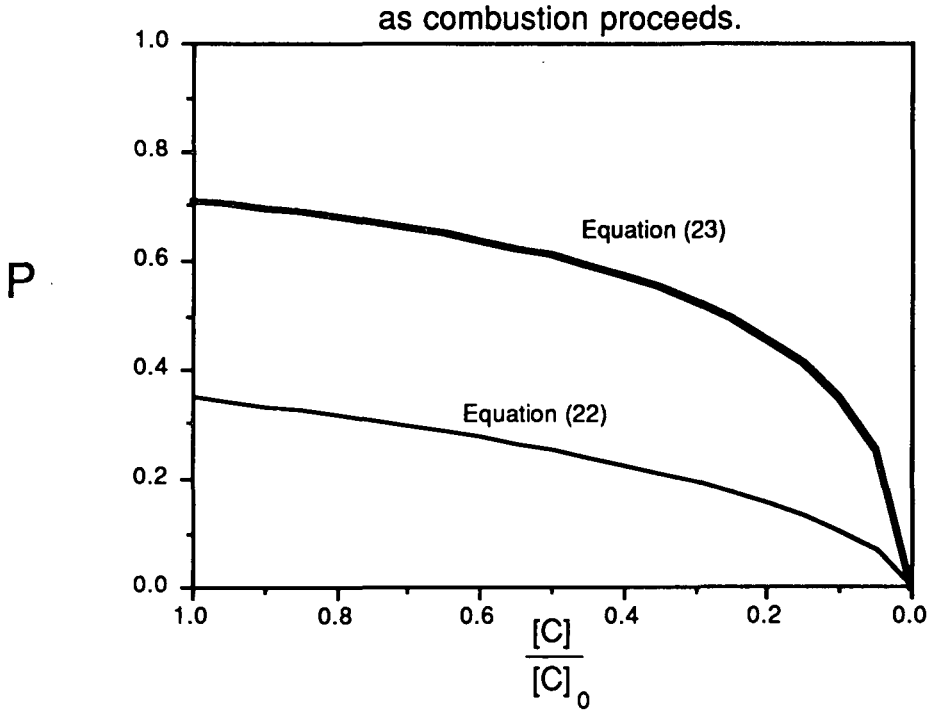

External surface area

The surface area of a sphere can be calculated from variables that are known as combustion proceeds. The volume of the particle, which is just the mass of the particle divided by the density, can be used to calculate the external surface area. The change in particle mass is due to carbon loss and oxygen loss/gain from the sulfate (weight change from fuming and sulfur loss are assumed to be negligible for now). Thus, the mass as a function of time is known from Equations (17) and (18), and the volume can be calculated as a function of mass by dividing the mass by a calculated density.

The change in density with mass loss is determined using the following concept of a char particle. Consider a char particle to be comprised of carbon, inorganic salts, and void volume. Assume that the char particle maintains its low density during combustion because of the strength of the carbon matrix; if this is true, it is reasonable to assume that the particle densification is related to the loss of strength of the matrix due to carbon loss. The density of the particle is

$$\rho_p = \frac{m_C + m_I}{V_C + V_I + V_{VOID}} \tag{24}$$

where the subscripts C and I denote carbon and inorganic. The volumes are calculated as the mass divided by the density, and the void volume is related to the amount of carbon left in the particle:

$$V_{VOID} = V_{VOID_0} \frac{m_C}{m_{C_0}} \tag{25}$$

The particle density becomes

$$\rho_p = \frac{m_C + m_I}{\frac{m_C}{\rho_C} + \frac{m_I}{\rho_I} + V_{VOID0} \frac{m_C}{m_{C_0}}} = \frac{m_C + m_I}{m_C \left(\frac{1}{\rho_C} + \frac{V_{VOID0}}{m_{C_0}} \right) + \frac{m_I}{\rho_I}} = \frac{m_C + m_I}{\frac{m_C}{\rho_{C_A}} + \frac{m_I}{\rho_I}} \tag{26}$$

where ρ_{C_A}, the "apparent" carbon density, is the reciprocal of the term in the parentheses. The volume of the particle is thus

$$V_p = \frac{m_C + m_I}{\rho_p} = \frac{m_C}{\rho_{C_A}} + \frac{m_I}{\rho_I} \tag{27}$$

At the end of the burn, the particle will still have a finite volume since char has a high ash content:

$$\frac{V_\infty}{V_0} = \frac{x_{inorganic}\, \rho_{char}}{\rho_{inorganic}} \tag{28}$$

where

$x_{inorganic}$ = mass fraction of inorganic in the char
$\rho_{inorganic}$ = density of the inorganic material (2 g/cc)
ρ_{char} = initial char density (assumed to be 0.2 g/cc).

Through extensive rearrangement, Equation (27) becomes:

$$\frac{V_p}{V_0} = \left(1 - \frac{V_\infty}{V_0}\right)\frac{[C]}{[C]_0} + \frac{V_\infty}{V_0} \tag{29}$$

Assuming a spherical geometry, the particle diameter is

$$d_p = d_{p_0}\left(\left(1 - \frac{V_\infty}{V_0}\right)\frac{[C]}{[C]_0} + \frac{V_\infty}{V_0}\right)^{\frac{1}{3}} \tag{30}$$

The external surface area is then πd_p^2.

Boundary Layer Calculations

The CO and CO_2 concentrations in the gas phase around the particle must be estimated in order to calculate R_{CO_2} from Equation (13). The estimates are obtained by doing a mass balance on the boundary layer. The boundary layer thickness is approximated by Equation (31):

$$\delta = 5\sqrt{\frac{\nu\, d_p}{U_\infty}} \tag{31}$$

where

δ = boundary layer thickness
ν = kinematic viscosity
d_p = particle diameter
U_∞ = velocity past particle

The approximate volume of the boundary layer is

$$V_{bl} = \frac{\pi\,(d_p + \delta)^3}{6} - \frac{\pi\, d_p^3}{6} \tag{32}$$

A CO_2 mass balance on the boundary layer gives:

$$R_{COX} + R_{CS} = F_{Dif} + R_{CO_2} + A_{CO_2} + F_{Conv} \quad (33)$$

where R_{COX} = C/O_2 rate
R_{CS} = C/SO_4 rate
R_{CO_2} = C/CO_2 rate
F_{Dif} = diffusion away from particle
F_{Conv} = convection away from particle
A_{CO_2} = accumulation of CO_2 in the boundary layer

Note that CO_2 can react only with a fraction of the surface equal to P since, as discussed earlier, the C/CO_2 reaction is much slower in smelt.

The concentration of the CO_2 in the boundary layer at any point in time is:

$$C_{CO_2} = \frac{M_{CO_2}}{V_{bl}} \quad (34)$$

where
C_{CO_2} = CO_2 concentration in the boundary layer
M_{CO_2} = mass of CO_2 in the boundary layer

Differentiating Equation (34) with respect to t gives:

$$\frac{d\,C_{CO_2}}{d\,t} = \frac{1}{V_{bl}}\frac{d\,M_{CO_2}}{d\,t} - \frac{M_{CO_2}}{V_{bl}^2}\frac{d\,V_{bl}}{d\,t} \quad (35)$$

Furthermore

$$A_{CO_2} = \frac{d\,M_{CO_2}}{d\,t} \quad (36)$$

A_{CO_2} can be solved for from Equation (33) and substituted into Equation (35) (via Equation (36)); $\frac{d\,V_{bl}}{d\,t}$ is solved for from Equation (37):

$$\frac{d\,V_{bl}}{d\,t} = \frac{V_{bl\,(t)} - V_{bl\,(t-1)}}{\Delta\,t} \quad (37)$$

Finally, the CO_2 concentration at each time step is calculated from the discretized form of the derivative:

$$C_{CO_2\,(t+1)} = C_{CO_2\,(t)} + \frac{d\,C_{CO_2}}{d\,t}\,\Delta t \qquad (38)$$

An analogous process is used to calculate the CO concentration.

SIMULATION PARAMETERS

The weight loss curve of a single kraft char particle burn can be used to test the model. The rate of mass loss of a kraft char particle was measured in a single particle reactor (3). The particle is suspended from a microbalance in a 5 x 5 cm duct through which a heated gas flows. The char is prepared by pyrolyzing a dried black liquor pellet in nitrogen. The residual char is then burned by introducing oxygen into the gas stream.

Experimental temperatures were not measured, so a temperature profile must be assumed for the model. The particle temperature is assumed to begin at the gas temperature and ramp linearly up to a maximum temperature after a period of time. This pattern is consistent with the pattern seen by Hupa in experimental char particle burns (1). Hupa found that the temperature of a particle in a muffle furnace increased in a fairly linear manner after pyrolysis until it reached a maximum temperature of 1200 °C near the end of burning. The temperature then trailed off. The experimental gas temperature for the IPC char burn was 1158 K, and the maximum particle temperature, T_{max}, is assumed to be 1473 K. The particle is assumed to begin at the experimental gas temperature and ramp linearly to the maximum temperature and stay there. The length of time to reach maximum temperature is a variable. Hupa found that T_{max} came near the end of char burning. For the IPC data, T_{max} is assumed to occur at thirteen seconds. The

IPC data, however, were obtained in a moving gas stream while Hupa's data were taken in a stagnant atmosphere, so the time to T_{max} is not necessarily the same. Although particle temperatures were not taken in the IPC data, visual observation suggests that the temperature rises rapidly upon contact with air, reaching a high temperature in a short time. The time to reach T_{max} is a variable. In this paper, six seconds and thirteen seconds were used as two assumed times to reach T_{max}.

RESULTS

A comparison between the model predictions and a kraft particle burn is shown in Figure 4. Four model prediction curves are shown. Equation (22) ("low P") and Equation (23) ("high P") were the two forms of the P function used, and six and thirteen seconds were assumed to be the times to reach T_{max}, yielding the four curves shown. The four curves will be discussed in the order shown in the legend of Figure 4. The "first" curve refers to the top line in the legend, proceeding in order to the fourth curve.

The first curve fits the data best. The initial portion of the first line is influenced by the particle heatup. Because the particle is relatively cool in the initial period, i.e., a relatively slow C/Na_2SO_4 rate, reduction efficiency starts to decrease. The weight loss due to carbon gasification is partially offset by the weight gained by net oxidation of sulfide. As the particle continues to heat, however, the reduction efficiency is regained until it approaches a high level. Then, the combustion appears to be mass-transfer limited, and the weight-loss rate becomes fairly linear. The reduction efficiency begins to decrease at about thirteen seconds since there is not much carbon left to maintain a high C/Na_2SO_4 rate. A gain of weight is seen after fifteen seconds as sulfide is oxidized by the air.

Figure 4. Model prediction vs. kraft char data.

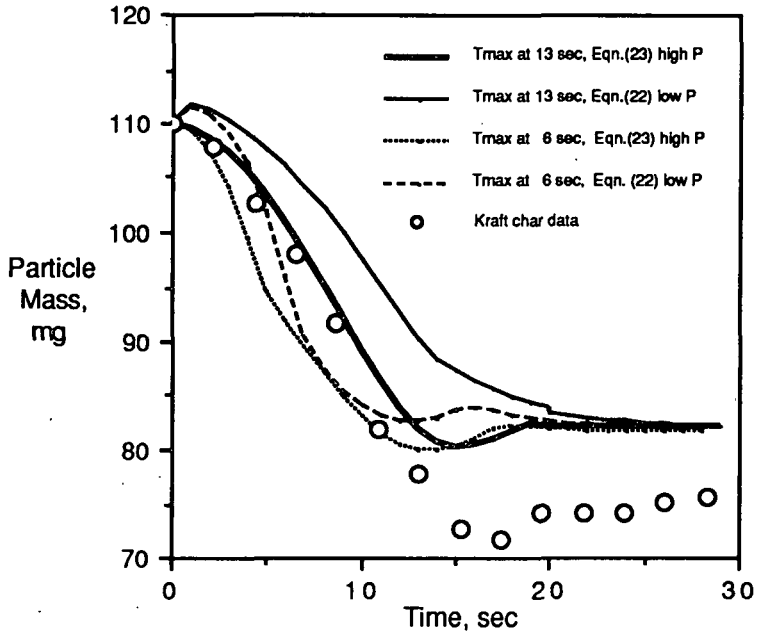

The first curve follows the data well until about ten seconds, after which the data fall below the model prediction. The model assumes that the sodium remains constant during burning; but fuming occurs during char burning, so the actual weight loss would tend to be greater than the prediction of the model. Another possible explanation for the weight-loss discrepancy has to do with the apparatus. The char particle hangs from a microbalance, and it is possible for small bits of char or smelt to break away from the particle as burning proceeds. This would also tend to make the actual mass loss greater than the model prediction. If the data points after ten seconds are moved up several mg, they are seen to follow the shape of the model prediction. Thus, if a small piece of char or smelt broke away between nine and ten seconds, the data after ten seconds could be moved up, resulting in a better fit between the model and the data. Both fuming and particle fragmentation will tend to make the actual weight

loss greater than the predicted curve although fuming is the more likely explanation.

The second curve is less successful in predicting the data. Equation (22) predicts a lower value for P throughout the burn than Equation (23). This means that more oxygen reacts via the sulfate/sulfide cycle, requiring a higher temperature to maintain a high reduction efficiency than if Equation (23) were used. The sulfide rapidly oxidizes in the beginning of the burn, and the particle actually gains weight since the rate of carbon mass loss is less than the rate of oxygen mass gain. The increasing temperature as combustion proceeds does not increase the C/Na_2SO_4 rate enough to obtain any net reduction of sulfate, so no weight gain is seen at the end of the burn.

The third and fourth lines are similar in shape. A small weight gain is seen at the beginning followed by a brief period of rapid weight loss due to net reduction of sulfate and carbon loss. A distinct transition to mass-transfer control is seen at about five and seven seconds as the weight-loss rate decreases to the rate of oxygen transfer to the particle. A fairly linear weight-loss rate persists until carbon is sufficiently depleted. Then oxidation of sulfide occurs.

The discrepancy between the first curve of Figure 4 and the data can be eliminated if moderate fuming is assumed. If a total of 10% of the inorganic material is emitted over the first fifteen seconds of the burn, the model prediction fits the data very well as shown in Figure 5. The prediction in Figure 5 uses the same conditions assumed for the first curve in Figure 4 with the addition of weight loss due to fuming.

Figure 5. Model prediction vs. kraft char data.

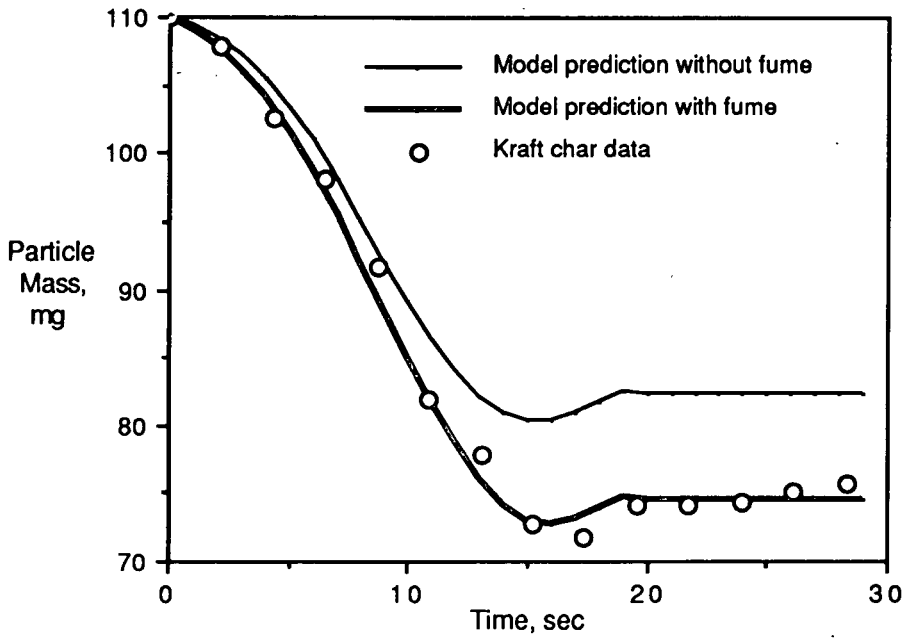

The relative amounts of CO and CO_2 are plotted in Figure 6. The fraction CO was an indefinite parameter in Grace's sulfate/sulfide cycle, but here it is an output of the model. CO is the dominant species while there is sufficient carbon present, but CO_2 predominates near the end of combustion when little carbon remains.

Figure 6. Relative amounts of carbon monoxide and carbon dioxide.

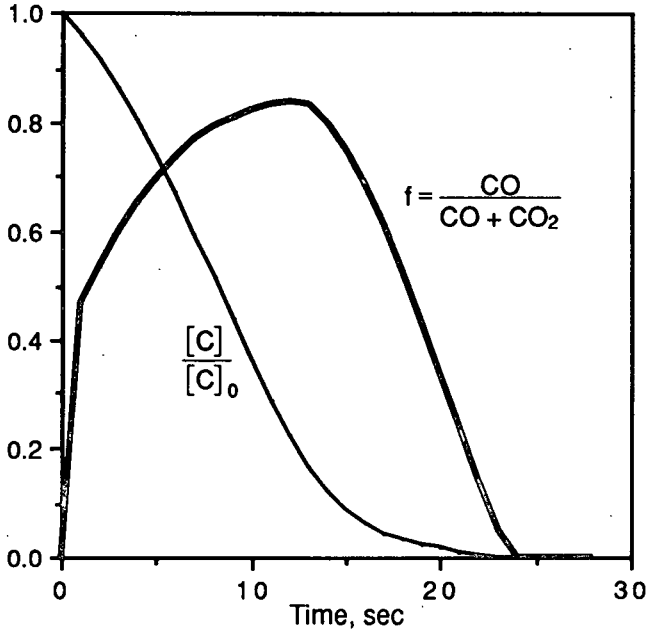

DISCUSSION

The parameters used to produce the most accurate prediction of the weight loss curve are consistent with experimental conditions and observations. The temperature profile (T_{max} at thirteen seconds) is consistent with Hupa's muffle furnace experiments in which the maximum temperature of 1473 K was reached near the end of the burn rather than near the beginning. In the case of the data simulated here, T_{max} at thirteen seconds represents a gradual heating period whereas T_{max} at six seconds represents a rapid heatup period followed by a sustained high temperature. A rapid heatup causes an initial period of weight loss due to sulfate reduction on top of carbon loss, causing the predicted weight to drop off more sharply than the data. On the other hand, a gradual heatup causes the initial portion of the weight loss prediction to be more gradual since the carbon loss is offset somewhat by sulfide oxidation.

The calculation of P with Equation (23) provided a more accurate simulation than the use of Equation (22). The implication of this result is that the C/O_2 reaction plays an important role in protecting the reduction efficiency by providing an alternate path for the oxygen to react with the char. Equation (23) predicts that more oxygen will go to the C/O_2 reaction to a greater extent of reaction than Equation (22). Conversely, Equation (22) predicts that more oxygen will oxidize sulfide at a lower extent of reaction. The reduction efficiency becomes increasingly vulnerable as combustion proceeds because more oxygen reacts with sulfide and because the carbon concentration decreases, causing a slower C/Na_2SO_4 rate.

Figure 6 is consistent with experimental results for the relative amounts of CO and CO_2. CO is the dominant species when significant amounts of char carbon is present. Aiken measured a CO fraction of 0.85 in char pile combustion experiments (10). On the other hand, CO_2 was the dominant species in the smelt pool reactor studies discussed earlier which used low carbon concentrations. This is consistent with Figure 6 after the carbon is nearly gone. CO_2 can only react directly with the char carbon. As combustion proceeds, more of the particle surface becomes molten, so less char carbon is in direct contact with the CO_2 in the gas phase. Thus, very little CO is produced when the carbon concentration is low.

CONCLUSIONS

The implications of the sulfate/sulfide cycle were discussed by Grace (3). The oxidation of char carbon and the reduction of sulfate are not mutually exclusive. It is possible to maintain a high reduction efficiency while carbon is burned if the reaction temperature is high enough. Oxygen need not be kept away from the bed; in fact, air should be supplied to the bed to meet the stoichiometric requirement of the material reaching the bed. The implications

of the sulfate/sulfide cycle provide an impetus to maximize bed burning in order to improve furnace operation by achieving a high reduction efficiency and reducing carryover.

The accuracy of the model prediction suggests that the combustion of char in an oxygen-rich atmosphere is adequately described by the rate equations discussed in this paper. The model describes the rate of char carbon combustion as well as the reduction efficiency during combustion -- two important process variables. Fuming cannot be neglected if an accurate weight loss prediction is desired, but it can be neglected if the only variables being calculated are the carbon combustion rate and the reduction efficiency.

The char burning model presented in this paper is an improvement of the sulfate/sulfide theory of char burning, and provides a framework for a general theory of char burning. It was here applied to particles, but it is general enough to be applied to other configurations. The equations can be applied to char bed geometries, and other reactions such as the C/H_2O reaction can be incorporated to model the overall bed behavior. The bed model would be able to predict how much burning is possible on the char bed as well as reduction efficiency. This work is underway as a Ph.D. thesis at The Institute of Paper Chemistry.

ACKNOWLEDGMENTS

Portions of this work were used by D.W.S. as partial fulfillment of the requirements for the Ph. D. degree at The Institute of Paper Chemistry.

LITERATURE CITED

1.) Hupa, M.; Solin, P. Combustion behavior of black liquor droplets. TAPPI Proceedings, 1985 International Chemical Recovery Conference, Book 3, p. 335.

2.) Gehri, R.; Oldenkamp, R. Status and economics of the Atomics International aqueous carbonate flue gas desulfurization process. FGD Symp. Proc. Rept. EPA-600/2-76-136A, May, 1976.

3.) Grace, T. M.; Cameron, J. H.; Clay, D. T. Role of sulfate/sulfide cycle in char burning -- experimental results and implications. TAPPI 69(10):108(1986).

4.) Smoot, L. D.; Smith, P. J. Coal Combustion and Gasification, Plenum Press, New York, 1985.

5.) Thorman, R. P.; Macur, T. S. Kinetics of sodium sulfate reduction by carbon in molten sodium carbonate. TAPPI Proceedings, 1985 International Chemical Recovery Conference, Book 3, p. 451.

6.) Cussler, E. L. Diffusion: Mass transfer in fluid systems. Cambridge University Press, 1984.

7.) Ranz, W. E., and Marshall, W. R., Chem. Eng. Prog., 48: 173(1952).

8.) Goerg, K., and Cameron, J. Kinetic study of kraft char gasification with carbon dioxide. AIChE Mtg.(Boston) Preprint no. 67g, 6p. (Aug 24-27) 1986.

9.) Li, J. M. Eng. Thesis, Chapter 3, McGill University, Montreal, Feb. 1986.

10.) Aiken, G. The use of a char pile reactor to study char bed processes. Doctoral Dissertation. Appleton, WI, The Institute of Paper Chemistry, January 1988.